J|A|C|S
ARTICLES
Published on Web 11/15/2006

Direct Measurements of Rate Constants and Activation Volumes for the Binding of H_2, D_2, N_2, C_2H_4, and CH_3CN to $W(CO)_3(PCy_3)_2$: Theoretical and Experimental Studies with Time-Resolved Step-Scan FTIR and UV−Vis Spectroscopy

David C. Grills,[†] Rudi van Eldik,[‡] James T. Muckerman,[†] and Etsuko Fujita*,[†]

Contribution from the Chemistry Department, Brookhaven National Laboratory, Upton, New York 11973-5000, and Institute for Inorganic Chemistry, University of Erlangen-Nürnberg, Egerlandstrasse 1, 91058 Erlangen, Germany

Received June 29, 2006; E-mail: fujita@bnl.gov

Abstract: Pulsed 355 nm laser excitation of toluene or hexane solutions containing **W**−L (**W** = *mer,trans*-$W(CO)_3(PCy_3)_2$; PCy_3 = tricyclohexylphosphine; L = H_2, D_2, N_2, C_2H_4, or CH_3CN) resulted in the photoejection of ligand L and the formation of **W**. A combination of nanosecond UV−vis flash photolysis and time-resolved step-scan FTIR (s^2-FTIR) spectroscopy was used to spectroscopically characterize the photoproduct, **W**, and directly measure the rate constants for binding of the ligands L to **W** to reform **W**−L under pseudo-first-order conditions. From these data, equilibrium constants for the binding of L to **W** were estimated. The UV−vis flash photolysis experiments were also performed as a function of pressure in order to determine the activation volumes, $\Delta V^{\ddagger}$, for the reaction of **W** with L. Small activation volumes ranging from −7 to +3 cm^3 mol^{-1} were obtained, suggesting that despite the crowded W center an interchange mechanism between L and the agostic W···H−C interaction of one of the PCy_3 ligands (or a weak interaction with a solvent molecule) at the W center takes place in the transition state. Density functional theory (DFT) calculations were performed at the B3LYP level of theory on **W** with/without the agostic C−H interaction of the PCy_3 ligand and also on the series of model complexes, *mer,trans*-$W(CO)_3(PH_3)_2L$ (**W′**−L, where L = H_2, N_2, C_2H_4, CO, or *n*-hexane) in an effort to confirm the infrared spectroscopic assignment of the **W**−L complexes, to simulate and assign the electronic transitions in the UV−vis spectra, to determine the nature of the HOMO and LUMO of **W**−L, and to understand the agostic C−H interaction of the ligand vs solvent interaction. Our DFT calculations indicate an entropy effect that favors agostic W···H−C interaction over a solvent σ C−H interaction by 8−10 kcal mol^{-1}.

Introduction

The efficient activation and conversion of small, stable molecules, such as H_2, N_2, CH_4, C_2H_4, and CO_2, into industrially useful, functionalized compounds via metal-mediated catalytic processes remains a key challenge for organometallic chemists in the 21st century. The successful development of such processes would provide major economic and environmental benefits. One of the key steps in these molecular activation processes involves the binding of the substrate molecule to a vacant coordination site at a transition-metal center. The kinetics and thermodynamics of this step can have a major effect on the overall mechanism and efficiency of the catalytic process. Therefore, it is vital that these binding steps are fully characterized and understood to allow the development of better and more efficient catalysts.

In 1983, Kubas and co-workers isolated the first example of a nonclassical molecular dihydrogen complex, *mer,trans*-$W(CO)_3(P^iPr_3)_2(\eta^2\text{-}H_2)$.[1−5] This was a remarkable discovery since it demonstrated an entirely new form of chemical bonding involving the donation of a σ-bonding electron pair to a vacant metal orbital. The family of $M(CO)_3(PR_3)_2(H_2)$ (M = Cr, Mo, W) complexes is now often referred to as the "Kubas complexes".[1] In $M-(\eta^2\text{-}H_2)$ the metal center stabilizes H_2 binding by back-donation from a filled d orbital to the empty σ^* orbital of the H−H bond.[1,6] Prior to this breakthrough, dihydrogen complexes were assumed to be unobservable intermediates in the oxidative addition of dihydrogen to form metal dihydrides. However, by systematic, mainly electronic, variations of the ligand set, a large series of dihydrogen complexes has since been isolated, each one exhibiting a different degree of H−H bond elongation and each representing a snapshot along the H−H bond activation pathway, ultimately leading to classical metal dihydride complexes.

[†] Brookhaven National Laboratory.
[‡] University of Erlangen-Nürnberg.

(1) Kubas, G. J. *Metal Dihydrogen and σ-Bond Complexes: Structure, Theory, and Reactivity;* Kluwer Academic/Plenum Publishers: New York, 2001.
(2) Kubas, G. J.; Ryan, R. R.; Swanson, B. I.; Vergamini, P. J.; Wasserman, H. J. *J. Am. Chem. Soc.* **1984**, *106*, 451−452.
(3) Kubas, G. J.; Unkefer, C. J.; Swanson, B. I.; Fukushima, E. *J. Am. Chem. Soc.* **1986**, *108*, 7000−7009.
(4) Kubas, G. J.; Ryan, R. R.; Wrobleski, D. A. *J. Am. Chem. Soc.* **1986**, *108*, 1339−1341.
(5) Wasserman, H. J.; Kubas, G. J.; Ryan, R. R. *J. Am. Chem. Soc.* **1986**, *108*, 2294−2301.
(6) Kubas, G. J. *Acc. Chem. Res.* **1988**, *21*, 120−128.

10.1021/ja064627e CCC: $33.50

Thermodynamic and kinetic parameters for the addition of small molecules such as H_2, D_2, and N_2, to **W** (**W** = *mer*,*trans*-W(CO)$_3$(PCy$_3$)$_2$ and PCy$_3$ = tricyclohexylphosphine), eq 1, have not been reported. However, Hoff's group elegantly employed stopped-flow kinetics[7,8] to measure the indirect substitution reaction of **W**−L (L = H_2 and N_2) with pyridine (py), evaluating $k_{f(H_2)}$ and $k_{f(N_2)}$ as $(2.2 \pm 0.3) \times 10^6$ and $(5.0 \pm 1.0) \times 10^5$ M^{-1} s^{-1}, respectively, at 25 °C. Since reaction 1 with L = py was too fast to follow under pseudo-first-order conditions on a stopped-flow apparatus, they first accurately determined the rate constant of reaction 1 with L = P(OMe)$_3$. On the basis of the substitution reaction mechanism and its rate law outlined in eqs 2 and 3, respectively, and $k_{2(P(OMe)_3)} = 5.45 \times 10^4$ M^{-1} s^{-1} in toluene at 25 °C, they calculated $k_{2(py)} = 8.7 \times 10^5$ M^{-1} s^{-1}.[7,8] Substitution reaction 4 was used for the evaluation of $k_{f(H_2)}$ and $k_{f(N_2)}$.

$$\mathbf{W} + \mathrm{L} \underset{k_{r(L)}}{\overset{k_{f(L)}}{\rightleftharpoons}} \mathbf{W}\text{−L} \quad (1)$$

$$\mathbf{W}\text{−py} \underset{k_{-2(py)}}{\overset{k_{2(py)}}{\rightleftharpoons}} \mathbf{W} + \mathrm{py} \xrightarrow[\mathrm{P(OMe)_3}]{k_{2(P(OMe)_3)}} \mathbf{W}\text{−P(OMe)}_3 \quad (2)$$

$$\frac{\mathrm{d}[\mathbf{W} - \mathrm{py}]}{\mathrm{d}t} = \frac{k_{2(py)}k_{2(P(OMe)_3)}[\mathbf{W} - \mathrm{py}][\mathrm{P(OMe)_3}]}{k_{-2(py)}[\mathrm{py}] + k_{2(P(OMe)_3)}[\mathrm{P(OMe)_3}]} \quad (3)$$

$$\mathbf{W}\text{−L} + \mathrm{py} \rightarrow \mathbf{W}\text{−py} + \mathrm{L} \quad (4)$$

Furthermore, they determined the enthalpies[9] for reaction 1 in toluene by solution calorimetry (−9.9, −13.5, −15.1, −18.9, −26.6, and −30.4 kcal mol^{-1} for L = H_2, N_2, CH_3CN, py, P(OMe)$_3$, and CO, respectively).

While the activation enthalpy ($\Delta H^{\ddagger}$) and entropy ($\Delta S^{\ddagger}$), and the overall enthalpy ($\Delta H°$) and entropy ($\Delta S°$) changes for these reactions using **W** and other complexes have been extensively investigated using both calorimetric and stopped-flow techniques, there is no information on the activation volume ($\Delta V^{\ddagger}$) for the formation of dihydrogen, dinitrogen, or ethylene complexes of **W** and other metal centers. Activation volumes describe the volume changes that occur along the reaction coordinate of a chemical process upon going to the transition state, and can provide further information on the underlying mechanism and the nature of the transition state, e.g. for small-molecule addition to **W** with highly bulky PCy$_3$ ligands. In the present study we report direct measurements of rate constants and activation volumes for the formation of **W**−L from **W** and L. When a toluene or hexane solution containing **W**−L (L = H_2, D_2, C_2H_4, N_2, or CH_3CN) and a known amount of L is irradiated with a 355 nm laser pulse, **W**−L bond dissociation takes place to form **W**. Subsequently, clean regeneration of **W**−L is observed using time-resolved UV−vis and step-scan FTIR (s^2-FTIR) spectroscopy. In addition, we have performed density functional theory (DFT) calculations at the B3LYP level of theory on **W** with/without the agostic C−H interaction of the PCy$_3$ ligand and also on a series of model complexes, *mer*,*trans*-**W′**−L (**W′** = W(CO)$_3$(PH$_3$)$_2$; L = H_2, C_2H_4, N_2, or CO) in an effort to resolve discrepancies between earlier spectral assignments[1,3,5,10] and our current IR observations, to simulate and assign the electronic transitions in the UV−vis spectra, to determine the nature of the HOMO and LUMO of **W**−L, and to understand the agostic C−H interaction of the ligand vs solvent σ C−H interaction.

Experimental Section

Materials. W was prepared as previously described[5] and characterized by NMR, UV−vis, and IR spectroscopy. No impurities were found in the NMR and IR spectra except for a trace amount of **W**−CO, which has previously been reported[5] to be present in solutions of **W**. CH_3CN and pyridine were purified in the published manner,[11] stored under vacuum over activated molecular sieves, and then vacuum-distilled and transferred in an Ar-filled glovebox just prior to sample preparation. THF was purified in the published manner[11] and stored under vacuum over NaK. Toluene and hexane were distilled over sodium benzophenone ketyl and CaH_2, respectively, under an Ar atmosphere and stored in the glovebox. Ultrahigh purity H_2, D_2, N_2, C_2H_4, CO, and Ar (Praxair) were used without further purification. The solubilities of the various gases in toluene and hexane were calculated from previously published data.[12] Accordingly, the following values at 25 °C and 1 atm partial pressure of gas are used in this study: $[H_2]$ = 2.97 and 4.80 mM in toluene and hexane, respectively; $[D_2]$ = 3.06 and 4.91 mM in toluene and hexane,[13] respectively; $[N_2]$ = 5.37 and 10.7 mM in toluene and hexane, respectively; $[C_2H_4]$ = 139 and 178 mM in toluene and hexane, respectively.

Spectroscopic Measurements. UV−vis spectra were measured on a Hewlett-Packard 8452A diode-array spectrophotometer. FTIR spectra were recorded on a Bruker IFS 66/S spectrometer. NMR spectra were measured on a Bruker UltraShield 400 MHz spectrometer. UV−vis flash photolysis experiments were conducted using an apparatus described previously,[14,15] with excitation being provided by the third harmonic (355 nm, ~6 ns, ~20 mJ/pulse) of a Continuum Surelite I-10 Nd:YAG laser. These experiments were performed in toluene at 25 °C under 1 atm of Ar or under a known pressure of H_2, D_2, N_2, C_2H_4, or CO. The solutions containing 0.1−0.5 mM **W**−py or 0.5−1.0 mM **W**−$NCCH_3$ were prepared using a known amount of py or CH_3CN, respectively, in a glovebox. The solutions containing 0.5−1.5 mM **W**−L (L = H_2, D_2, N_2, C_2H_4 or CO) were prepared by adding a known pressure of L after having degassed the Ar-saturated toluene solution of **W**. The kinetics of the signal-averaged data were analyzed using Levenberg−Marquardt nonlinear least-squares routines written in MATLAB. For the high-pressure work, the solution containing **W**−L (L = H_2, N_2, or C_2H_4) was transferred via a syringe into a vacuum-tight quartz pillbox optical cell,[16−18] which had been flushed with H_2, N_2, or C_2H_4 as in previous investigations.[18,19] The solution containing **W**−py or **W**−$NCCH_3$ was transferred in a similar manner under Ar. After removing the excess gas, the pillbox was immediately placed inside the high-pressure cell, which was mounted on the laser table.

(7) Zhang, K.; Gonzalez, A. A.; Hoff, C. D. *J. Am. Chem. Soc.* **1989**, *111*, 3627−3632.
(8) Gonzalez, A. A.; Zhang, K.; Hoff, C. D. *Inorg. Chem.* **1989**, *28*, 4285−4290.
(9) Gonzalez, A. A.; Zhang, K.; Nolan, S. P.; Delavega, R. L.; Mukerjee, S. L.; Hoff, C. D.; Kubas, G. J. *Organometallics* **1988**, *7*, 2429−2435.
(10) Bender, B. R.; Kubas, G. J.; Jones, L. H.; Swanson, B. I.; Eckert, J.; Capps, K. B.; Hoff, C. D. *J. Am. Chem. Soc.* **1997**, *119*, 9179−9190.
(11) Riddick, J. A.; Bunger, W. B.; Sakano, T. K. *Organic Solvents: Physical Properties and Methods of Purification*, 4th ed.; Wiley: New York, 1986.
(12) Wilhelm, E.; Battino, R. *Chem. Rev.* **1973**, *73*, 1−9.
(13) Since we could not find any published data on the solubility of D_2 in hexane, this value has been estimated by scaling the solubility of H_2 in hexane according to the relative solubilities of D_2 and H_2 in heptane.
(14) Hamada, T.; Brunschwig, B. S.; Eifuku, E.; Fujita, E.; Korner, M.; Sasaki, S.; van Eldik, R.; Wishart, J. F. *J. Phys. Chem. A* **1999**, *103*, 5645−5654.
(15) Thompson, D. W.; Wishart, J. F.; Brunschwig, B. S.; Sutin, N. *J. Phys. Chem. A* **2001**, *105*, 8117−8122.
(16) le Noble, W. J.; Schlott, R. *Rev. Sci. Instrum.* **1976**, *47*, 770−771.
(17) van Eldik, R. High-Pressure Kinetics: Fundamental and Experimental Aspects. In *Inorganic High-Pressure Chemistry: Kinetics and Mechanisms*; van Eldik, R., Ed.; Elsevier: Amsterdam, 1986; Vol. 7, pp 8−11.
(18) Fujita, E.; van Eldik, R. *Inorg. Chem.* **1998**, *37*, 360−362.
(19) Fujita, E.; Brunschwig, B. S.; Creutz, C.; Muckerman, J. T.; Sutin, N.; Szalda, D.; van Eldik, R. *Inorg. Chem.* **2006**, *45*, 1595−1603.

Time-resolved step-scan FTIR experiments were performed by operating the Bruker IFS 66/S FTIR spectrometer in step-scan mode and using the third harmonic of the Nd:YAG laser to excite the sample at a repetition rate of 5 Hz (Laser master/FTIR slave). A 1 mm photovoltaic HgCdTe infrared detector equipped with a 20 MHz preamplifier (Kolmar, KMPV11-1-LJ2/239) was used in these experiments. The detector has both AC- and DC-coupled outputs, which were amplified and/or attenuated by external preamplifiers and attenuators (Phillips Scientific, model nos. 6931 and 5010 and Stanford Research Systems, SR560) and digitized by an external 100 MHz 8-bit digitizer (Spectrum, PAD82a). Before commencing the laser excitation measurement, the DC output was collected in step-scan mode with Mertz phase correction, to generate a set of single beam background spectra and also to store a set of phase spectra in memory, which were later used to automatically phase correct the subsequent time-resolved AC spectra. During the laser measurement, the AC output was monitored and amplified by $\times 10-20$, to use the full dynamic range of the digitizer. Optical band-pass filters (OCLI, W05342-8 ca. 2000−1765 cm^{-1} band-pass and W04944-8 ca. 2260−1830 cm^{-1} band-pass) were used in order to minimize the number of interferogram mirror positions. Single-sided interferograms, with 4 or 8 laser shots at each mirror position, were collected at a spectral resolution of 4 cm^{-1}, and a phase resolution of 32 cm^{-1}. Delta absorbance TRIR spectra, $\Delta(OD)_t$, at each of the 100 time delays, t following the laser flash, were generated using the equation, $\Delta(OD)_t = -\log_{10}(1 + \gamma(AC)_t/DC)$, where γ is the ratio of the amplifications applied to the DC and AC signals, $(AC)_t$ is the single-beam spectrum generated from the detector's AC output at time t after the laser flash and DC is the single-beam spectrum that was generated from the DC output before the laser measurement. Due to intense absorptions of toluene in the metal carbonyl infrared region, the s^2-FTIR experiments were performed in 25−50 mL of hexane, at a concentration of ca. 0.5 mM. The dry, degassed, violet-colored hexane solutions of **W** were saturated with a known pressure of the appropriate gas, L, in order to generate **W**−L, which typically had a pale-yellow color. The solutions were handled in an air-sensitive manner and flowed cyclically through an airtight, home-built flow system consisting of 1/8 in. o.d. stainless steel tubing and Swagelok fittings, a glass sample reservoir vessel fitted with glass-to-metal 1/4 in. Kovar joints, a 1 mm path length CaF_2 IR flow cell (Harrick Scientific Products, DLC-S25), and a recirculating gear pump (Micropump, GA-V23JFSG with HG-0024 drive).

DFT Calculations. Gas-phase DFT calculations on the series of model complexes, *mer*,*trans*-**W′**−L (L = none, H_2, C_2H_4, N_2, CO, or *n*-hexane), and on **W** and $W(CO)_3(PH_3)(PH_2Cy)$ with and without an agostic interaction, were carried out using the hybrid B3LYP method[20−22] and the Hay−Wadt VDZ (n+1) ECP (LANL2DZ ECP) basis set for W[23−25] and the 6-31G** (5d) basis set for H, C, N, O, and P.[26−28] Note that the computed "net agostic interaction energy" discussed in this paper is the sum of the intrinsic agostic interaction energy and any steric and/or electronic energy differences associated with the two different conformers. Although this is not the intrinsic "agostic" interaction, it is nevertheless a relevant number. Geometry optimizations and frequency analyses were performed using the Gaussian 03 package of programs.[29] Time-dependent B3LYP calculations were carried out with the Gaussian 03 program in order to predict the UV−vis spectra of the various species. Calculated geometries are shown in Table 3 and Figures 4 and 5, and binding energies are summarized in Table 4.

Table 1. UV−Vis and FTIR Spectroscopic Properties Observed for **W**−L Complexes in Toluene and Hexane, Respectively, at 25 °C

L	properties
	UV−vis[a]
none	312 (9700), 350 sh (830), 452 sh (900), 566 (1100)
none[b]	452 sh, 550
H_2	366 (1300), 390 sh (1100)
N_2	350 sh (2400), 370 (2500), 408 (3300)
C_2H_4	350 sh (3200), 400 sh (1300)
CH_3CN	340 sh (3200), 430 sh (1300), 485 sh (540)
CO	346 (2500), 382 (3000)
py	560 (6600)
	IR[c]
none	1819m, 1837s, 1949w
H_2	1847s, 1851s, 1861s, 1912w, 1963w, 1988w
D_2	1847s, 1851s, 1860s, 1908w, 1965w, 1988w
N_2	1853s, 1857sh, 1953w, 2113w (ν_{NN}),2117w (ν_{NN})
C_2H_4	1841s, 1865m, 1962w
CO	1866s, 1871vw, sh

[a] λ_{max}, nm (ϵ, M^{-1} cm^{-1}) in toluene. [b] In THF. [c] ν(CO), cm^{-1} in hexane, s = strong, m = medium, w = weak, sh = shoulder, v = very.

Results

UV−Vis Spectra of W and W−L Species. When an appropriate gas L (L = H_2, N_2, C_2H_4, CO) was added at a partial pressure of 1 atm to a degassed violet solution containing **W** at room temperature, the 566 nm absorption of **W** completely disappeared due to the high stability of the **W**−L species being formed (eq 1). The final solution is yellow as reported previously.[5] UV−vis spectra of **W** and **W**−L are summarized in Table 1 and shown in Figure 1. Upon removal of the gases, such as H_2, N_2 and C_2H_4, by freeze−pump−thaw cycles from the solutions containing the corresponding **W**−L species in toluene or THF, the original **W** spectra were cleanly reproduced. However, CO binding in **W**−CO was found not to be reversible. In the case of **W**−py (py = pyridine), upon addition of py, the 566 nm absorption is replaced by a much more intense absorption band at 560 nm, and the solution turned bright red.

Flash Photolysis. Flash photolysis experiments on **W**−L in toluene were carried out using 355 nm pulsed laser excitation. Figure 2 shows the transient absorption spectrum of a short-lived species observed 2 μs after excitation of a toluene solution containing 1.40 mM **W**−C_2H_4 at 25 °C at an ethylene partial pressure of 740 Torr. By comparison with the UV−vis spectrum of **W** in Figure 1, this transient species can easily be assigned to **W**, which is then observed to decay as **W**−L is reformed under pseudo-first-order conditions. Similar transient spectra were also observed for L = H_2, D_2, N_2, or CH_3CN. The observed pseudo-first-order rate constant for the reformation process is given by eq 5.

$$k_{obs} = k_f[L] + k_r \quad (5)$$

The forward and reverse rate constants (k_f and k_r in eqs 1 and 5) in toluene were determined at 25 °C. Figure 3 shows a plot of the observed rate constants for formation of **W**−L (L = H_2 and D_2) as a function of H_2 and D_2 concentration in toluene. The slopes and intercepts of these plots yield $k_f = (2.0 \pm 0.1) \times 10^6$ M^{-1} s^{-1} and $k_r = 950 \pm 100$ s^{-1} for L = H_2, and $k_f = (1.6 \pm 0.1) \times 10^6$ M^{-1} s^{-1} and $k_r = 680 \pm 70$ s^{-1} for L = D_2.

(20) Becke, A. D. *Phys. Rev. A* **1988**, *38*, 3098−3100.
(21) Lee, C.; Yang, W.; Parr, R. G. *Phys. Rev. B.* **1988**, *37*, 785−789.
(22) Miehlich, B.; Savin, A.; Stoll, H.; Preuss, H. *Chem. Phys. Lett.* **1989**, *157*, 200−206.
(23) Hay, P. J.; Wadt, W. R. *J. Chem. Phys.* **1985**, *82*, 270−283.
(24) Wadt, W. R.; Hay, P. J. *J. Chem. Phys.* **1985**, *82*, 284−298.
(25) Hay, P. J.; Wadt, W. R. *J. Chem. Phys.* **1985**, *82*, 299−310.
(26) Ditchfield, R.; Hehre, W. J.; Pople, J. A. *J. Chem. Phys.* **1971**, *54*, 724−728.
(27) Hehre, W. J.; Ditchfield, R.; Pople, J. A. *J. Chem. Phys.* **1972**, *56*, 2257−2261.
(28) Hariharan, P. C.; Pople, J. A. *Theor. Chim. Acta* **1973**, *28*, 213−222.
(29) Pople, J. A.; et al. *Gaussian 03*, revision B.04; Gaussian, Inc.: Wallingford CT, 2004.

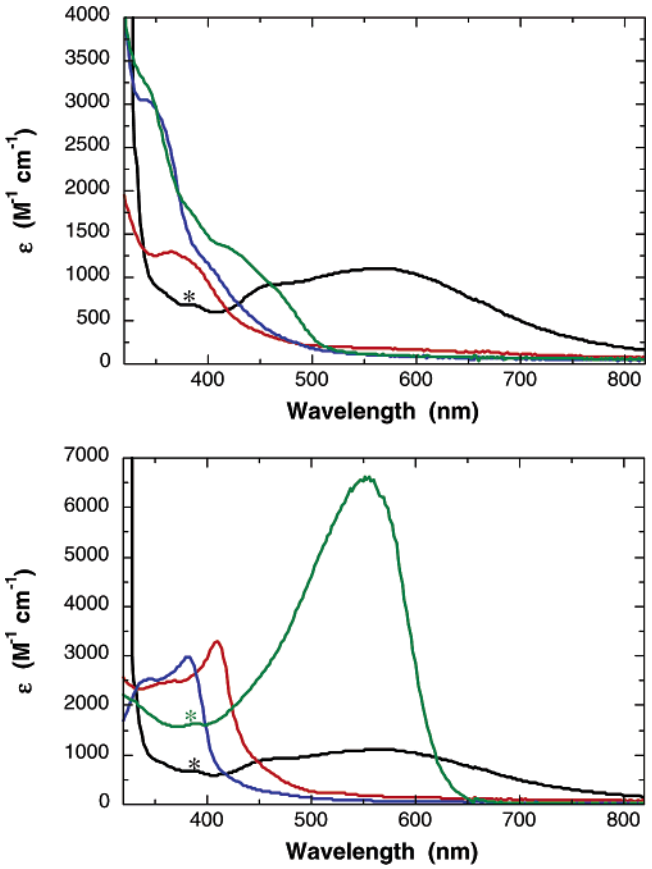

Figure 1. UV−vis spectra of various **W**−L complexes in toluene: (top) **W**, black; **W**−H_2, red; **W**−C_2H_4, blue; and **W**−$NCCH_3$, green; (bottom) **W**, black; **W**−N_2, red; **W**−CO, blue; and **W**−py, green; * = minor contamination by **W**−CO.

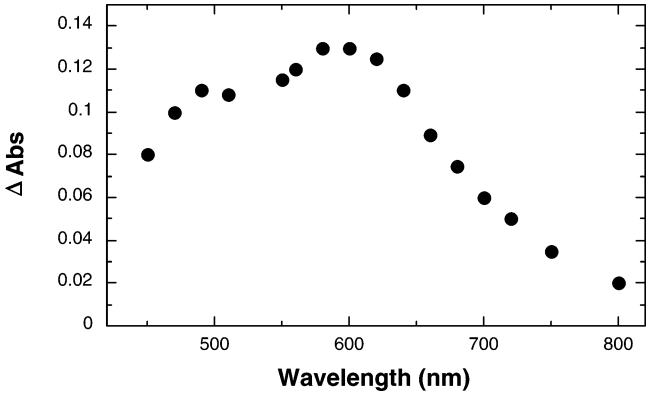

Figure 2. Transient absorption spectrum obtained 2 μs after 355 nm pulsed laser excitation of a solution containing 1.4 mM **W**−C_2H_4 and 740 Torr C_2H_4 in toluene at 25 °C.

The equilibrium constants, K calculated from k_f/k_r for **W**−H_2 and **W**−D_2 are thus 2100 and 2300 M^{-1}, respectively. Figures S1−S3 (Supporting Information) show plots of the observed rate constants for the formation of **W**−L (L = N_2, C_2H_4, CH_3CN) as a function of the concentration of L in toluene. The forward and reverse rate constants and the equilibrium constants for **W**−L, calculated in a similar manner, are summarized in Table 2.

Activation Volumes. The forward rate constants for the formation of **W**−L (eq 1) in toluene were determined as a function of pressure at 25 °C. Since the contribution of k_r to

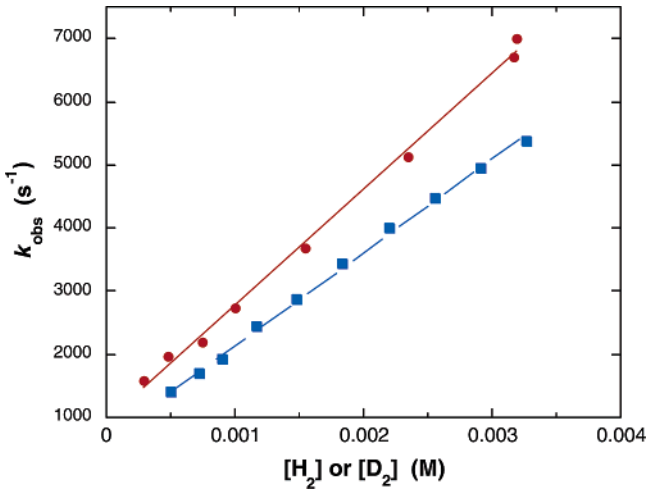

Figure 3. Plot of observed rate constants for formation of **W**−H_2 (red) and **W**−D_2 (blue) as a function of gas concentration in toluene at 25 °C. $[H_2]$ = 2.97 mM/atm, $[D_2]$ = 3.06 mM/atm at 25 °C.

k_{obs} is small, it can be assumed that $k_f[L] \approx k_{obs}$ under the experimental conditions used. The effect of pressure on the relaxation process was found to be reproducible for a complete pressure cycle, i.e. increasing pressure from ambient to 2000 atm and decreasing the pressure back to ambient conditions. A relatively small increase or decrease in the rate was observed in all cases (Table S1, Supporting Information). The activation volume, $\Delta V^{\ddagger}(k_f)$, was estimated from the initial slope ($= -\Delta V^{\ddagger}/RT$) of the plot of $\ln(k_{obs})$ vs pressure, and the results are included in Table 2. The activation volumes range from −7 $cm^3\ mol^{-1}$ for C_2H_4 to +3 $cm^3\ mol^{-1}$ for CH_3CN.

DFT Calculations: Geometric and Electronic Structures and Vibrational Analyses. The optimized Cartesian coordinates for *mer*,*trans*-**W′**−L (L = none, H_2, C_2H_4, N_2, CO, or *n*-hexane), **W** with and without an agostic interaction, and $W(CO)_3(PH_3)(PH_2Cy)$ with and without an agostic interaction are presented in Tables S2−S13 (Supporting Information). The calculations on **W′**−L were performed mainly in an effort to confirm our assignment of three ν(CO) bands in the IR spectra of the **W**−L complexes under study. This is due to a discrepancy that exists over the assignment of these ν(CO) bands in the literature[1,3,5,10] vs the spectra measured in this work. For example, while our IR experiments for **W**−C_2H_4 clearly show three ν(CO) bands, Wasserman et al. only reported two of these.[5] Bender et al.[10] also missed one of the three ν(CO) bands[30,31] in their normal-coordinate analysis of **W**−H_2, probably based on previously reported experimental values (1963 and 1843 cm^{-1}).[3,5] In accordance with previous theoretical and experimental studies,[32] our DFT calculations show that the ligand, L in *mer*,*trans*-**W′**−L, and hence presumably in **W**−L, is oriented parallel to the P−W−P axis for L = H_2 and C_2H_4 (see Figure 4, b and f). For L = N_2, the dinitrogen molecule binds end-on via a single N atom, which is a common coordination mode for N_2 (see Figure 4e).[33−35] (However, N_2 can act as a bridging ligand to form dimeric species such as $(P^iPr_3)(CO)_3W-N_2-W(CO)_3((P^iPr_3)$, the structure of which has been solved.[47]) In further

(30) Tomas, J.; Lledos, A.; Jean, Y. *Organometallics* **1998**, *17*, 190−195.
(31) Tomas, J.; Lledos, A.; Jean, Y. *Organometallics* **1998**, *17*, 4932−4939.
(32) Kubas, G. J. *J. Organomet. Chem.* **2001**, *635*, 37−68.
(33) Hidai, M.; Mizobe, Y. *Chem. Rev.* **1995**, *95*, 1115−1133.
(34) Leigh, G. J. *Acc. Chem. Res.* **1992**, *25*, 177−181.
(35) Yandulov, D. V.; Schrock, R. R. *Science* **2003**, *301*, 76−78.

Table 2. Reaction Rate Constants, Equilibrium Constants (calculated from k_f/k_r) and Activation Volumes for the Formation of **W**−L with Various Ligands, L, Using UV−Vis Flash Photolysis at 25 °C or Step-Scan FTIR Spectroscopy at 23 ± 2 °C

ligand	solvent	method	k_f, M^{-1} s^{-1}	k_r, s^{-1}	calcd K, M^{-1}	$\Delta V^{\ddagger}$, cm^3 mol^{-1}
H_2	toluene	UV−vis	$(2.0 \pm 0.1) \times 10^6$	950 ± 100	2100 ± 300	-3 ± 1
H_2	hexane	s^2-FTIR	[a] 3×10^6			
D_2	toluene	UV−vis	$(1.6 \pm 0.1) \times 10^6$	680 ± 70	2300 ± 300	
D_2	hexane	s^2-FTIR	[a] 2×10^6			
C_2H_4	toluene	UV−vis	$(3.4 \pm 0.3) \times 10^4$	570 ± 70	60 ± 10	-7 ± 1
C_2H_4	hexane	s^2-FTIR	$(7 \pm 1) \times 10^4$			
N_2	toluene	UV−vis	$(3.0 \pm 0.2) \times 10^5$	99 ± 10	3000 ± 350	-3 ± 1
N_2	hexane	s^2-FTIR	[a] 3×10^5			
CH_3CN	toluene	UV−vis	$(3.6 \pm 0.3) \times 10^6$	<200	$>2 \times 10^4$	$+3 \pm 1$

[a] These rate constants were estimated from a single experiment at one concentration of ligand, L using the equation, $k_f = (k_{obs} - k_r)/[L]$, where k_{obs} is the observed rate of decay of the photoproduced **W** and k_r is the reverse rate constant that we obtained by UV−vis flash photolysis in toluene.

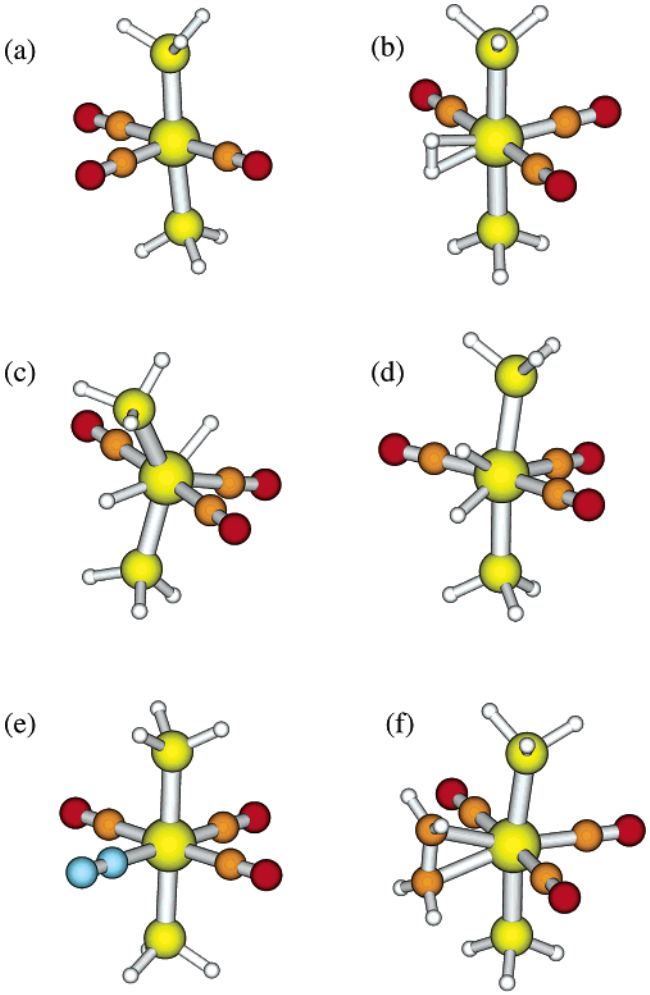

Figure 4. DFT optimized structures of (a)**W′**, (b) **W′**−H_2 (dihydrogen), (c) **W′**−$(H)_2$ (*distal* dihydride complex), (d) **W′**−$(H)_2$ (*cis*-dihydride complex), (e) **W′**−N_2 and (f) **W′**−C_2H_4.

agreement with previous theoretical studies,[30,31] our DFT calculations establish that the H ligands in the lowest-energy configuration of the dihydride form (**W′**−$(H)_2$) are arranged in a *distal* fashion, either side of one of the PH_3 ligands (see Figure 4c), as opposed to remaining in a *cis* orientation (Figure 4d), which might otherwise have been anticipated following a simple elongation of the H−H bond during the oxidative addition process. While we used a slightly different basis set for the geometry optimizations, our results on the electronic energies without zero-point energy corrections (ΔE) and geometries of the three species (**W′**−H_2, **W′**−*distal*-$(H)_2$, and **W′**−*cis*-$(H)_2$) are in agreement with results published previously.[30,31] The free energies ($\Delta G°_{298}$) for the formation of **W′**−H_2, **W′**−*distal*-$(H)_2$, and **W′**−*cis*-$(H)_2$ are −6.5, −1.2, and −0.1 kcal mol^{-1}, respectively (See Table 4). The corresponding three sets of ν(CO) bands were calculated and are shown in Figure 8b.

Calculations on **W**, **W′**, **W′**−*n*-hexane, $W(CO)_3(PH_3)(PH_2Cy)$, and $W(CO)_3(PCy_3)(PH_3)$ were carried out to investigate the strength of an agostic interaction of a C−H of a PCy_3 ligand vs the hydrocarbon solvent interaction. Figures 4a and 5a−e show optimized geometries of these complexes. In the five-coordinate square pyramidal, **W′**, the basic structural features of **W′**−L remain the same except that a large unoccupied d_{z^2} orbital exists on the opposite side of the unique CO with a shorter W−CO distance (1.934 Å) than those calculated for other **W′**−L complexes (av 2.020 Å). We calculated the geometric and electronic structure of **W′**−*n*-hexane to compare with **W′**: the shortest W−H and W−C distances are 2.208 and 3.025 Å, respectively and the **W′**−*n*-hexane electronic (ΔE) and free ($\Delta G°_{298}$) energies of formation are −5.4 and +5.3 kcal mol^{-1}, respectively. Furthermore, geometry optimizations were performed for both the agostic and nonagostic $W(CO)_3(PH_3)(PH_2Cy)$ complexes (where nonagostic refers to a local minimum-energy structure in a conformation that does not allow an agostic W···H−C interaction from the Cy group): the shortest W−H and W−C distances are 2.217 and 3.242 Å, respectively, in the agostic complex and 3.472 and 4.065 Å, respectively, in the nonagostic complex. The calculated gas-phase net agostic interaction (ΔE) and free energy ($\Delta G°_{298}$) are −0.5 and +1.3 kcal mol^{-1}. The difference is small due to a small entropic contribution associated with the intramolecular interaction. Geometry optimizations were also performed for both the agostic and nonagostic **W** complexes: the shortest W−H and W−C distances are 2.488 and 3.206 Å, respectively, in the agostic complex and 3.196 and 3.812 Å, respectively, in the nonagostic complex. The calculated gas-phase net agostic interaction (ΔE) and free energy ($\Delta G°_{298}$) are −4.7 and −5.2 kcal mol^{-1}. The difference is again small due to a small entropic contribution associated with the intramolecular interaction. We should also point out that while an agostic α-C−H interaction was observed in both the X-ray structure and the DFT calculations for **W** and $W(CO)_3(PCy_3)(PH_3)$, respectively, an agostic β-C−H interaction was observed in the DFT calculations for $W(CO)_3(PH_3)(PH_2Cy)$ (Figure 5).

The DFT calculations also allow the nature of the HOMO and LUMO of **W**−L to be determined. Our DFT calculations

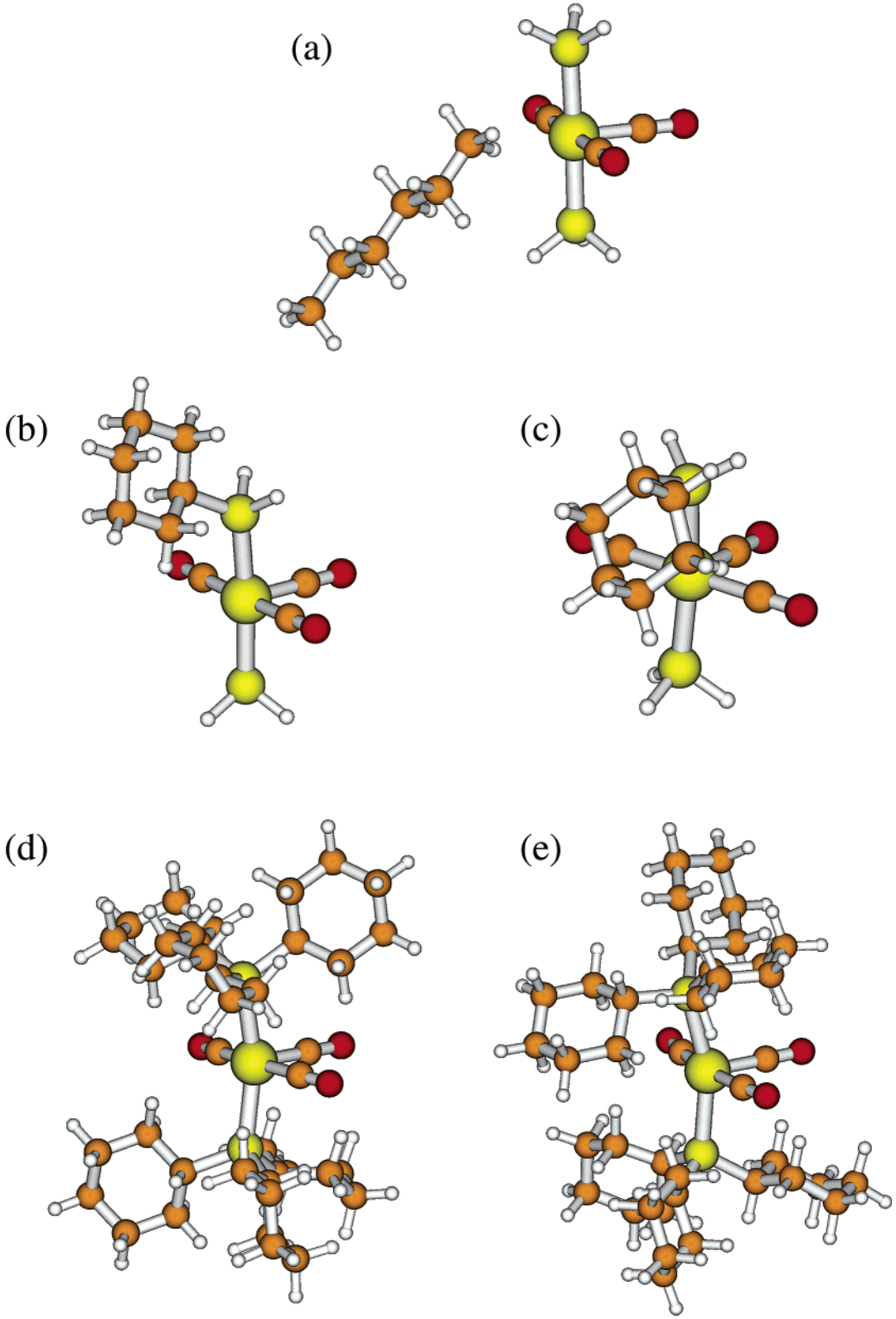

Figure 5. DFT optimized structures of (a) **W′**−*n*-hexane, (b) $W(CO)_3(PH_3)(PH_2Cy)$ without a C−H agostic interaction of Cy, (c) $W(CO)_3(PH_3)(PH_2Cy)$ with a C−H agostic interaction of Cy, (d) **W** without a C−H agostic interaction of PCy_3, and (e) **W** with a C−H agostic interaction of PCy_3.

on **W′**−N_2 have been published previously.[36] DFT calculations on **W′**−L (L = H_2, C_2H_4 and CO) show that the HOMO is mainly metal-based and that the LUMO is largely located on the three CO ligands and L, with some contribution of P* as shown in Table 3, Figure 6 and Figure S5. This general result suggests that the lowest-energy transition observed in the UV−vis spectra of **W**−L (see Figure 1) is metal-to-ligand charge transfer (MLCT) in nature. In the case of the five-coordinate **W′**, while the HOMO is dπ mixed with the unique CO*, the LUMO is dσ (d_{z^2}) mixed with the *trans* CO* (Figure 6).

(36) Grills, D. C.; Huang, K.-W.; Muckerman, J. T.; Fujita, E. *Coord. Chem. Rev.* **2006**, *250*, 1681−1695.

Table 3. DFT Calculated Geometrical Parameters for *mer,trans*-$W(CO)_3(PH_3)_2L$ (**W′**−L) Model Complexes

properties	**W′**	**W′**–H_2	**W′**–*distal*-$(H)_2$	**W′**–(C_2H_4)	**W′**–N_2	**W′**–CO
HOMO[a]	dπ + (CO*)	dπ + (CO*)	dπ + (CO*)	dπ + (CO*)	dπ + (CO*)	dπ + (CO*)
LUMO[a]	d_{z^2} + (CO*)	CO* + (P* + H_2*)	CO* + H^-* + P*	C_2H_4* + CO* + (P*)	N_2* + CO* + P*	CO* + (P*)
W−L (H_2, H^-, C_2H_4, N_2) distance, Å	−	1.908	1.752	2.396	2.110	−
H−H distance, Å	−	0.837	3.355	−	−	−
C−C (C_2H_4) distance, Å	−	−	−	1.403	−	−
N−N distance, Å	−	−	−	−	1.121	−
W−P distance, Å	2.457	2.466	2.469	2.465	2.468	2.473
W−CO (1) distance, Å	1.934	1.995	2.042	2.011	2.005	2.047
W−CO (2) distance, Å	2.039	2.040	2.035	2.037	2.046	−
C−O (1) distance, Å	1.172	1.163	1.155	1.162	1.164	1.159
C−O (2) distance, Å	1.161	1.160	1.160	1.161	1.159	−
P−W−P angle, deg	175.14	178.01	139.55	172.20	179.19	180.00
P−W−C (1) angle, deg	92.43	89.00	134.69	86.10	90.40	90.00
P−W−C (2) angle, deg	90.02	90.03	88.18	90.15	90.01	−
[b]ν(CO), cm^{-1}	1898(38)	1927(25)	1933(7)	1917(14)	1934(9)	1940(4359)[c]
	1919(91)	1941(9)	1973(2)	1937(6)	1938(5)	1974(6)
	1999(1)	2009(1)	2029(1)	2002(1)	2006(1)	2035(1)
[b]ν(HH), cm^{-1}		2846				
[b]ν(NN), cm^{-1}					2184	

[a] The orbitals in parentheses are minor contributions. [b] Frequencies scaled by 0.9613 (relative intensities for ν(CO)). [c] This band comprises two overlapping bands with almost identical frequencies and intensities.

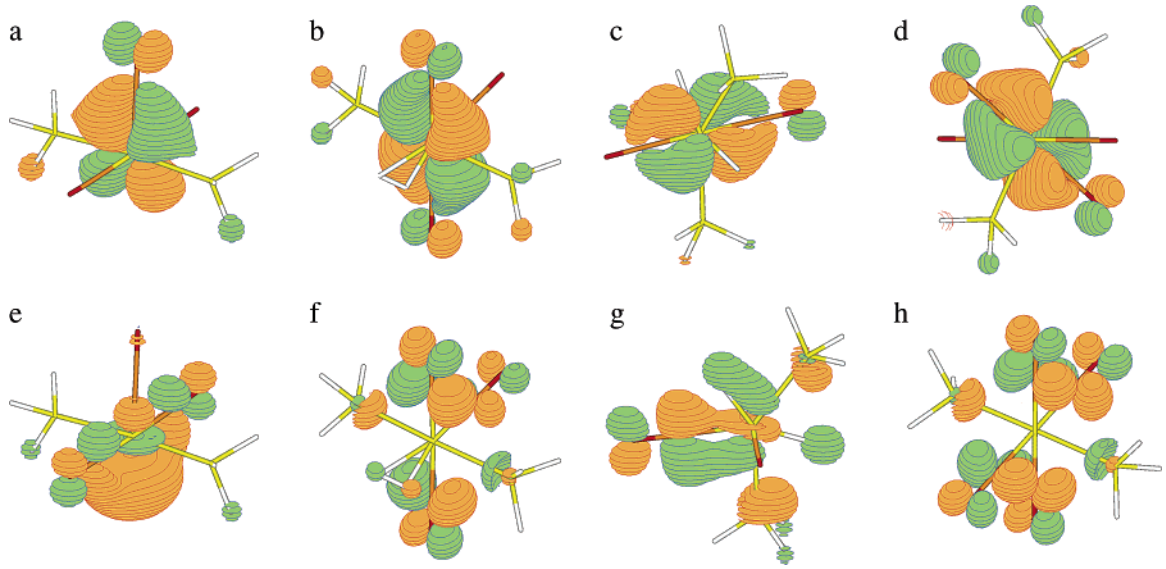

Figure 6. HOMO and LUMO for **W′** (a and e), **W′**−dihydrogen (b and f), **W′**−*distal* dihydride (c and g), and **W′**−CO (d and h), respectively.

Time-dependent DFT (TDDFT) calculations were carried out for the **W′**−H_2 and **W′**−$(H)_2$ (*distal*- and *cis*-dihydride) complexes because both the η^2-dihydrogen and the dihydride forms of **W**−H_2 exist in equilibrium in solution.[7,10] The UV−vis spectrum of **W**−H_2 in toluene shows an absorption band at 366 nm with a shoulder at 390 nm. TDDFT calculated spectra for **W′**−H_2 (blue curve), **W′**−*distal*-$(H)_2$ (red curve) and **W′**−*cis*-$(H)_2$ (green curve), shown in Figure 7a, indicate that λ_{max} of the lowest-absorption band of the **W′**−$(H)_2$ complexes (∼290 nm) is considerably blue-shifted compared to that of **W′**−H_2 (∼335 nm). The calculated absorptions for **W′**−H_2 are at higher energies than the experimental data, probably due to the electronic and steric effects caused by replacing PCy_3 with PH_3. However, the shape of the spectrum matches well with the observed spectrum. The lowest-energy transition is the HOMO−1 to LUMO excitation mixed with substantial HOMO−1 to LUMO+2 and HOMO−2 to LUMO+3 contributions at 340 nm, with an oscillator strength of 0.0059. The next lowest transition is the HOMO−1 to LUMO+1 excitation at 335 nm, with an oscillator strength of 0.0109. The third lowest transition is the HOMO to LUMO+2 excitation mixed with substantial HOMO−2 to LUMO+1 and HOMO to LUMO contributions at 301 nm, with an oscillator strength of 0.0141. Our theoretical investigation on **W′**−N_2 has been published previously.[36] In **W′**−C_2H_4, the lowest-energy transition is the HOMO to LUMO excitation mixed with a substantial HOMO−1 to LUMO+1 contribution at 373 nm with an oscillator strength of 0.0006 (See Figure S5 for the Frontier orbitals). The next lowest transition is the HOMO−2 to LUMO excitation mixed with substantial HOMO−2 to LUMO+2 and HOMO−1 to LUMO+3 contributions at 333 nm with an oscillator strength of 0.0105. The third lowest transition is the HOMO to LUMO+2 excitation mixed with substantial HOMO−1 to LUMO+1 and HOMO to LUMO contributions at 327 nm with an oscillator strength of 0.0039. The calculated absorptions are again at slightly higher energies, however, the shape of the spectrum matches well with the observed spectrum.

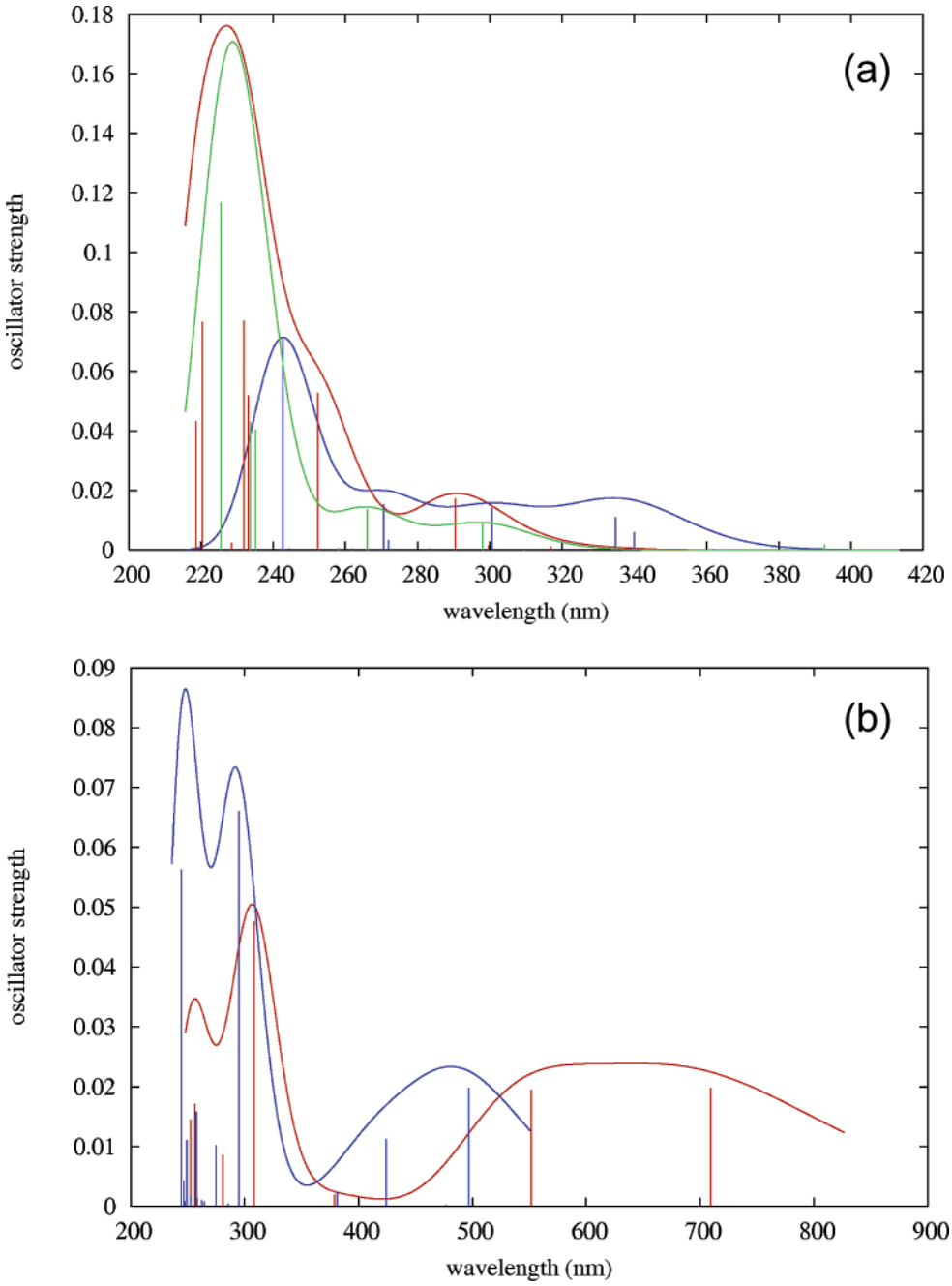

Figure 7. Calculated UV−vis spectra with oscillator strengths: (a) **W′**−dihydrogen (blue), **W′**−*distal*-dihydride complex (red) and **W′**−*cis*-dihydride complex (green); (b) **W′** (red) and **W′**−*n*-hexane (blue). The line spectra were converted with a Gaussian broadening function with a width parameter of 0.18 eV to obtain the continuous spectra shown.

We also conducted TDDFT calculations on the **W′** and **W′**−*n*-hexane complexes in the gas phase to understand the nature of the transition and the spectral change due to a weak solvent (such as a hexane) interaction. The results are shown in Figure 7b. The lowest transition in **W′** (red curve in Figure 7b) is the HOMO to LUMO excitation at 709 nm with an oscillator strength of 0.0198. The next lowest transition is the HOMO−2 to LUMO excitation mixed with a substantial HOMO−1 to LUMO+1 contribution at 551 nm with an oscillator strength of 0.0195. The third lowest transition is the HOMO−1 to LUMO+1 excitation mixed with a substantial HOMO−2 to LUMO+2 contribution at 309 nm with an oscillator strength of 0.0476. The calculated absorptions are in this case at slightly lower energies; however, the shape of the spectrum matches well with the observed spectrum in toluene. This could be due to this being a gas-phase calculation without any solvent interaction at the sixth coordination site. To prove this, we calculated the spectrum of **W′**−*n*-hexane (Figure 7b, blue curve). The lowest transition is the HOMO to LUMO transition at 497 nm with an oscillator strength of 0.0198. The second lowest transition is the HOMO−2 to LUMO excitation mixed with the HOMO−1 to LUMO+1 excitation at 424 nm with an oscillator strength of 0.0112. The calculated spectrum is shifted to a significantly higher energy than that of the experimental spectrum in either toluene or hexane. The experimental spectra of **W** in toluene and *n*-hexane are identical with λ_{max} at 566 nm. However, in THF λ_{max} is at 550 nm. The high-energy shift in the calculated spectra is

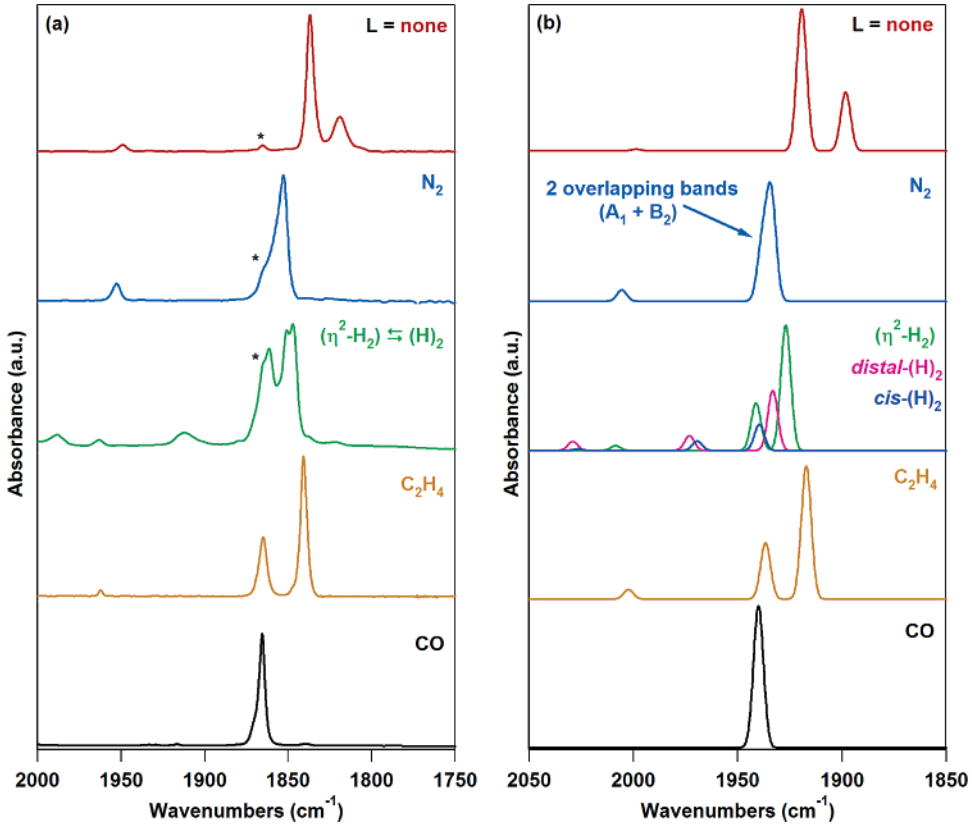

Figure 8. (a) Experimental IR spectra for five **W**−L complexes in hexane solution and (b) gas-phase DFT calculated IR spectra for five **W′**−L complexes. The calculated line spectra were converted with a Gaussian broadening function with a width parameter of 3.6 cm^{-1}. * = minor contamination by **W**−CO.

observed for all **W′**−L (L = H_2, N_2,[36] C_2H_4, *n*-hexane) complexes and could be due to the different electronic effect of PH_3 relative to that of PCy_3, combined with the fact that these are gas-phase calculations.

Figure 8a shows the experimentally observed FTIR spectra of **W** and **W**−L (L = N_2, H_2, C_2H_4, or CO) in hexane solution. The DFT calculated gas-phase IR spectra of the **W′**−L model complexes are shown in Figure 8b and summarized in Table 3. Since DFT with the B3LYP functional typically overestimates vibrational frequencies, the frequencies of the calculated spectra have been scaled by a factor of 0.9613, in accordance with an earlier recommendation[37] for the B3LYP functional when used with the 6-31G* basis set. As expected, the absolute frequency scale is still predicted too high since the calculations were performed on PH_3 complexes in the gas phase, as opposed to on PCy_3 complexes in hexane solution. However, the relative frequencies and intensities (see Table 3 and Figure 8) of the bands are in excellent agreement with our experimental results, thus confirming the presence of three ν(CO) bands in the IR spectra of **W**−L. For the H_2 complex, three additional ν(CO) bands are observed and calculated, due to the presence of the *cis*- and *distal*-dihydride complexes, which are in equilibrium with the η^2-dihydrogen σ-bonded species. It is clear from Figure 8 that *trans*-$W(CO)_4(PCy_3)_2$ exhibits a single, intense ν(CO) band that almost coincides with the middle of the three ν(CO) bands of the **W**−L complexes.

Step-Scan FTIR Spectroscopy. In all of the s^2-FTIR experiments, at least two of the ν(CO) bands of **W** (at 1837 and 1819 cm^{-1}) were observed as newly formed positive features immediately following photoexcitation of the **W**−L complex. In some cases the third, much weaker band of **W** was also observed at 1949 cm^{-1} if a negative bleach band of **W**−L was not obscuring it. The ν(CO) bands of **W** were then observed to decay exponentially via pseudo-first-order kinetics at the same rate as the recovery of the negative bleach bands of **W**−L during the reaction of **W** with excess L present in the solution. Some extremely minor, static features were observed in the baselines of the s^2-FTIR spectra, between ca. 1940 and 1900 cm^{-1}. These features are assigned to long-lived products associated with the photodecomposition of *trans*-$W(CO)_4(PCy_3)_2$, which is a minor, unavoidable contaminant in the samples.

Using the reverse rate constants, k_r that were measured in the UV−vis flash photolysis experiments in toluene (eq 1, Table 2), the forward rate constants, k_f for the s^2-FTIR experiments in hexane under a single partial pressure of L were estimated from $k_f = (k_{obs} - k_r)/[L]$, where k_{obs} is the observed rate of decay of the photogenerated **W** or observed rate of recovery of **W**−L, and [L] is the concentration of L. Despite the fact that it was necessary to perform the s^2-FTIR experiments in hexane rather than in toluene (due to intense IR absorption bands of toluene in the ν(CO) region), the rate constants estimated by s^2-FTIR are in reasonable agreement with those obtained by UV−vis flash photolysis in toluene (see Table 2). Band positions and rate constants for all of the complexes studied by s^2-FTIR are reported in Tables 1 and 2.

The FTIR spectrum of **W**−C_2H_4 in hexane under 1.8 atm partial pressure of C_2H_4 exhibits three ν(CO) bands at 1962, 1865, and 1841 cm^{-1} (Figure 9a). The s^2-FTIR spectra obtained at 2 μs intervals following 355 nm excitation of this solution

(37) Wong, M. W. *Chem. Phys. Lett.* **1996**, *256*, 391−399.

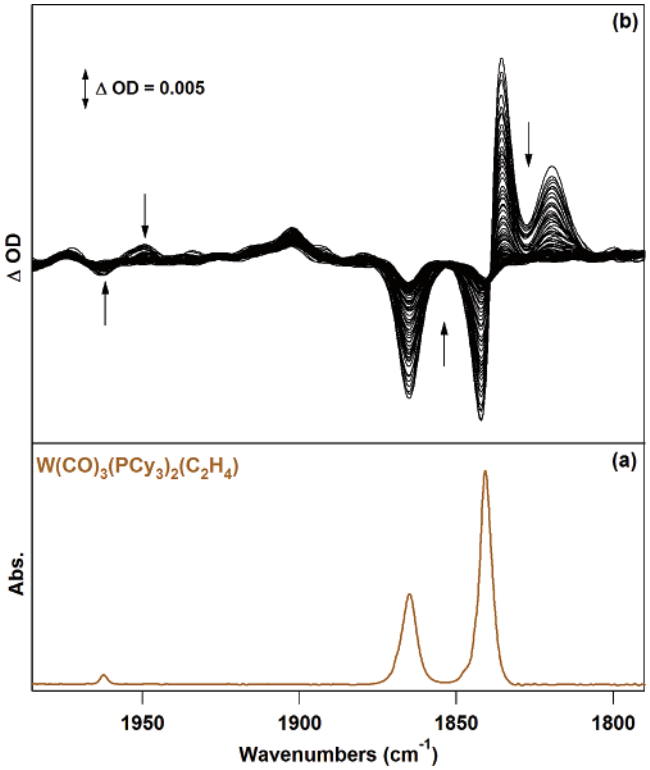

Figure 9. (a) FTIR of **W**−C_2H_4 in hexane under 1.8 atm partial pressure of C_2H_4, (using hexane saturated with 1.8 atm of C_2H_4 as a background spectrum). (b) Step-scan FTIR spectra recorded between 2 and 192 μs following 355 nm excitation of this solution. Arrows show directions of band decay and recovery following excitation.

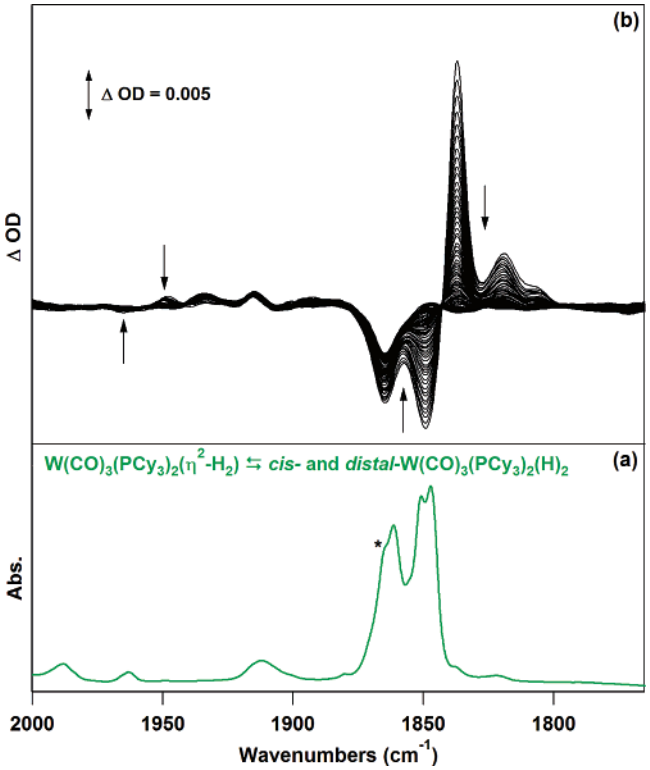

Figure 10. (a) FTIR of **W**−H_2 in hexane under 1.8 atm partial pressure of H_2, showing six overlapped ν(CO) bands due to the equilibrium mixture of **W**−(H_2), **W**−*distal*-$(H)_2$ and **W**−*cis*-$(H)_2$; * = minor contamination by **W**−CO. (b) Step-scan FTIR spectra recorded between 2 and 192 μs following 355 nm excitation of this solution. Arrows show directions of band decay and recovery following excitation.

are shown in Figure 9b. Three ν(CO) bands of **W**−C_2H_4 are observed to deplete, together with the simultaneous formation of the three characteristic bands of **W** at 1949, 1837, and 1819 cm^{-1}. A minor, static baseline artifact, which does not change in intensity throughout the duration of the experiment, is also observed at 1902 cm^{-1}. The transient ν(CO) bands of **W** are observed to decay exponentially at a rate ($k_{obs} = (2.3 \pm 0.2) \times 10^4$ s^{-1}) identical to the rate of recovery ($k_{obs} = (2.2 \pm 0.2) \times 10^4$ s^{-1}) of **W**−C_2H_4. The value of $k_{f(C_2H_4)}$ estimated (as described above) from this experiment was ca. 2× higher than that obtained by UV−vis flash photolysis of **W**−C_2H_4 in toluene. Therefore, the s^2-FTIR experiment was repeated at five different concentrations of C_2H_4 in order to more accurately determine $k_{f(C_2H_4)}$ for the reaction of **W** with C_2H_4 to reform **W**−C_2H_4 in hexane. The observed rate of decay, k_{obs}, of the photogenerated **W** complex varies linearly with respect to $[C_2H_4]$ (see Figure S4) and from the slope of this graph, $k_{f(C_2H_4)}$ was found to be $(7 \pm 1) \times 10^4$ M^{-1} s^{-1}.

For the dihydrogen adduct of **W**, the experiment is complicated by the presence of both the η^2-dihydrogen and the two dihydride forms of **W**−H_2, all of which exist in equilibrium with one another in solution. It has previously been estimated[7,10] that ca. 10−30% of **W**−H_2 in solution is present in the dihydride forms. This equilibrium gives rise to the six ν(CO) bands that are observed in the IR spectrum of **W**−H_2 in hexane and which were described earlier. In addition to the ν(CO) modes, the η^2-dihydrogen complex should exhibit six additional IR active modes involving the H_2 ligand, one of which is a ν(HH) stretching vibration.[10] The ν(HH) mode, which occurs at 2690 cm^{-1}, is extremely weak and broad and has only been clearly observed in Nujol mulls for complexes containing perdeuteriophosphine ligands, due to interference by the ν(CH) modes of the PCy_3 ligands and common solvents.[3,10] The five remaining **W**−H_2 vibrations are typically weak or medium in intensity and occur at frequencies significantly lower than those of the ν(CO) bands. As mentioned above, the dihydride species exists in equilibrium. However, **W**−hydride vibrations are very weak and lower in frequency than ν(CO). For these reasons, only the ν(CO) vibrations were probed in the present s^2-FTIR experiments. By comparison with our DFT calculations and previously published data,[3] the bands observed at 1963, 1861, and 1847 cm^{-1} are assigned to the η^2-dihydrogen complex and those at 1988, 1912, and 1851 cm^{-1} to the *distal*-dihydride species that exists in equilibrium with the dihydrogen complex in solution. According to our DFT calculations, the bands for the *cis*-dihydride species, which is the least stable of the hydrides, will overlap with the bands at 1988, 1912, and 1861 cm^{-1}. The slightly unsymmetrical shape of the band at 1912 cm^{-1} and the calculated bond energy suggest the existence of the *cis*-dihydride species, however, we expect that this is a minor species.

Upon 355 nm excitation of a hexane solution of **W**−H_2 saturated under 1.8 atm partial pressure of H_2, the ν(CO) bands at 1963 and 1861−1847 cm^{-1} are observed to bleach together with the concomitant formation of the three characteristic bands of **W** (see Figure 10). However, the dihydride bands at 1988 and 1912 cm^{-1} are not observed to bleach throughout the experiment, which suggests that 355 nm excitation selectively dissociates dihydrogen from the η^2-dihydrogen complex, leaving the dihydride complexes intact. Since only the η^2-dihydrogen complex is bleached upon 355 nm excitation, the dihydrogen/

dihydride complex equilibrium will be significantly perturbed immediately following the laser pulse. However, conversion from the dihydride complexes to the η^2-dihydrogen complex has previously been estimated to occur on a significantly longer time scale (τ = 30 ms for **W**−H_2 and τ = 16 ms for the ^{i}Pr analogue)[7,38] than that being probed in our experiments. Therefore, any interconversion between the dihydride and η^2-dihydrogen complexes would be far too slow to contribute to the measured kinetics. The conversion from the *cis*-dihydride species may be faster, but the contribution from this minor species has not been observed in our experiments. The transient ν(CO) bands of **W** decay exponentially at a rate (k_{obs} = (2.7 ± 0.3) × 10^4 s^{-1}) identical to the recovery rate (k_{obs} = (2.4 ± 0.2) × 10^4 s^{-1}) of the **W**−H_2 bands. However, on the time scale of this experiment, the bleach at 1861 cm^{-1} only partially recovers (by ca. 50%) and then remains constant. We assign this to the overlap of the 1861 cm^{-1} band of the dihydrogen complex, **W**−H_2, with the ν(CO) band of the *trans*-W(CO)$_4$(PCy$_3$)$_2$ (**W**−CO) contaminant. The *cis*-dihydride species also has a band which overlaps the 1861 cm^{-1} band of **W**−H_2, but the contribution should be almost negligible. The long-lived component of the bleach is likely to be associated with the photochemistry of *trans*-W(CO)$_4$(PCy$_3$)$_2$, which we are currently in the process of investigating and which will be the subject of a future report.

Analogous results were obtained for the s^2-FTIR of **W**−D_2 in the presence of 1.8 atm partial pressure of D_2. **W**−D_2 exhibits six ν(CO) bands in hexane solution at frequencies almost identical to those observed for the η^2-dihydrogen/dihydride complexes. These correspond to the η^2-dideuterium and the dideuterido forms of **W**−D_2, which exist in equilibrium with one another in solution. The ν(DD) stretching vibration of **W**−D_2 has previously been observed[10] by Raman spectroscopy as an extremely weak and broad feature at ca. 1900 cm^{-1}. However, in the IR spectrum it is obscured by the ν(CO) band at 1908 cm^{-1} and could not be probed by s^2-FTIR. Similar to the results obtained with **W**−H_2, only the ν(CO) bands corresponding to the η^2-dideuterium complex were observed to bleach upon excitation. The average lifetime for the decay of **W** and the regeneration of **W**−D_2 ($\tau \approx 47$ μs) in the s^2-FTIR of **W**−D_2 is slightly longer than that observed for the decay of **W** and the regeneration of **W**−H_2 ($\tau \approx 44$ μs) in the s^2-FTIR of **W**−H_2.

Our experimental investigation with step-scan FTIR and UV−vis techniques on **W**−N_2, together with a theoretical investigation of **W′**−N_2, has been published previously.[36]

Discussion

UV−vis Spectra of W−L. Whereas the FTIR and NMR spectra of **W**−L species have been extensively investigated,[1] their UV−vis spectra have rarely been discussed. Only the UV−vis spectrum of **W** in toluene has been previously reported.[5] The visible spectra of **W** in toluene and hexane are practically identical, showing λ_{max} at 566 nm with a shoulder at 452 nm. A small peak/shoulder at 384 nm is due to minor contamination by **W**−CO. However, λ_{max} in THF shifts to 550 nm, and the shoulder at 452 nm is less pronounced, indicating that THF weakly coordinates to the W center as suggested previously.[5] By contrast, there is no clear evidence for such coordination in toluene and hexane. We calculated UV−vis spectra of the **W′** complex without any agostic C−H interaction and **W′**−*n*-hexane in the gas phase. The lowest-energy absorption of the **W′** complex without any agostic C−H interaction and of **W′**−*n*-hexane is a d$\pi \rightarrow$ dσ transition heavily mixed with CO*. The second transition in both species is a metal-to-ligand charge transfer (MLCT) transition (dπ to CO*) mixed with some contribution of the d$\pi \rightarrow$ dσ transition. The lowest-energy absorption of all **W**−L complexes is MLCT in nature, i.e. a dπ (with small contribution of L* and CO*) $\rightarrow$ L* + CO* transition. Upon pulsed laser excitation into this band, the weak **W**−L bond cleaves and the **W** species forms. The transient UV−vis and FTIR spectra obtained 2 μs after excitation in toluene and hexane are identical to those of **W** as shown in Figures 1, 2, 8, 9, and 10. The formation of **W**−L from **W** and L was directly observed, and all reactions (L = H_2, D_2, N_2, C_2H_4, and CH_3CN) are cleanly first-order in [L]. The second-order rate constants (k_f) for the reaction between **W** and L (L = H_2, D_2, N_2) in toluene obtained by UV−vis detection are in good agreement with the values estimated by s^2-FTIR detection in hexane.

FTIR of W−L. Three IR-active ν(CO) bands ($2A_1 + B_2$) are expected to be observed for the *mer*,*trans*-W(CO)$_3$(PCy$_3$)$_2$L complexes in accordance with their C_{2v} symmetry (see Table 1). The $A_1(1)$ mode is the highest in frequency and extremely weak, but is observable due to coupling with the $A_1(2)$ mode and geometric distortions from the ideal *mer*,*trans* environment.[39] The results of the frequency analysis in our DFT calculations confirm that the $A_1(2)$ mode is the next lowest in frequency and of medium intensity. Finally, the B_2 mode is the most intense of the three and occurs at the lowest frequency. When this family of **W**−L complexes was initially reported,[40] three ν(CO) bands were identified in their IR spectra. However as described earlier, **W**−CO is generally present to a varying degree in samples of **W**−L due to a disproportionation reaction and/or minor oxidation. The single, intense ν(CO) band of **W**−CO almost coincides with the $A_1(2)$ band of the **W**−L complexes. For example, in hexane it is less than 0.5 cm^{-1} higher in frequency than the $A_1(2)$ mode of **W**−C_2H_4. In subsequent publications the $A_1(2)$ band of the **W**−L complexes has always been dismissed as merely a contamination by **W**−CO, and only two of the ν(CO) bands ($A_1(1)$ and B_2) have since been reported and assigned for these complexes.[1,3,5,10] Our DFT calculations have now confirmed the expected presence and relative intensities of all three IR-active ν(CO) modes for **W**−L (Figure 8 and Table 1). The agostic species, **W** also has C_{2v} symmetry and exhibits three ν(CO) bands, similar to the **W**−L complexes (see Figure 8 and Table 1). However, the intensity ratio of these bands is different from that of **W**−L. Despite the fact that it is not possible to model the agostic interaction using PH_3 ligands, the relative frequencies and intensities of the IR bands predicted by the DFT calculations agree well with the experimental IR spectrum of **W**.

In the s^2-FTIR experiment performed on **W**−H_2, only the ν(CO) bands that correspond to the η^2-dihydrogen complex were observed to bleach upon 355 nm excitation, while those of the dihydride species were unaffected. The photoejection of dihy-

(38) Khalsa, G. R. K.; Kubas, G. J.; Unkefer, C. J.; Vandersluys, L. S.; Kubat-Martin, K. A. *J. Am. Chem. Soc.* **1990**, *112*, 3855−3860.
(39) Braterman, P. S. *Metal Carbonyl Spectra*; Academic Press: London, 1975.
(40) Kubas, G. J. *J. Chem. Soc., Chem. Commun.* **1980**, 61−62.

drogen from transition-metal dihydride complexes is a well-known phenomenon and is a commonly used technique for the generation of reactive unsaturated species.[41−43] However, all known examples of such photoelimination reactions occur with *cis*-dihydrides. As discussed earlier, the results of our and previous[30,31] DFT calculations suggest that two dihydride complexes exist: one with the H ligands in a *cis* geometry and the other in a *distal* geometry with the H ligands separated by one of the PCy_3 ligands. The latter species is 0.7 kcal mol^{-1} more stable in our DFT calculations. The *distal* geometry may prevent the photoelimination of dihydrogen from the dihydride complex. However, it is possible that neither dihydride species may absorb the 355 nm laser light. To consider the possibility that neither dihydride species is excited by the 355 nm laser pulse, we carried out TDDFT calculations to investigate the UV−vis spectra of the dihydrogen and dihydride complexes of **W′**, which are shown in Figure 7a. The calculated spectrum of the **W′**−dihydrogen complex is blue-shifted compared to the experimental spectrum of the **W**−dihydrogen complex. However, this is a general trend of TDDFT calculations and is also due to the substitution of PCy_3 by PH_3 in the calculations. Since the calculated absorption bands of both **W′**−dihydride complexes are much more blue-shifted, the **W**−dihydride complexes likely do not absorb the 355 nm laser light. These calculated results are consistent with the observed transient FTIR spectra in our s^2-FTIR experiment performed on **W**−H_2.

Comparison of Binding Rate and Equilibrium Constants. The second-order rate constant for the reaction of acetonitrile with **W**, $k_{f(CH_3CN)} = (3.6 \pm 0.3) \times 10^6$ M^{-1} s^{-1}, is the highest among the reactions we and others[8] have measured for this series of complexes. However, it is still only a factor of 2 larger than that for H_2 and D_2. Hoff's group evaluated $k_{f(H_2)}$ and $k_{f(N_2)}$ as $(2.2 \pm 0.3) \times 10^6$ and $(5.0 \pm 1.0) \times 10^5$ M^{-1} s^{-1}, respectively.[7] Our directly measured values, $k_{f(H_2)} = (2.0 \pm 0.1) \times 10^6$ M^{-1} s^{-1} and $k_{f(N_2)} = (3.0 \pm 0.2) \times 10^5$ M^{-1} s^{-1} are similar to theirs, but slightly lower. The rate constant for the formation of **W**−H_2 in toluene is ca. 60× higher than that for the formation of **W**−C_2H_4, mainly due to the small size of H_2 compared to that of C_2H_4, and therefore there is a decreased steric interaction between the incoming ligand and the bulky PCy_3 ligands. Furthermore, this smaller steric repulsion is a major factor contributing to the greater stability of **W**−H_2 compared to that of **W**−C_2H_4. Using the s^2-FTIR technique, $k_{f(C_2H_4)}$ in hexane was determined to be $(7 \pm 1) \times 10^4$ M^{-1} s^{-1}, which is ca. 2× higher than the value, $k_{f(C_2H_4)} = (3.4 \pm 0.3) \times 10^4$ M^{-1} s^{-1}, measured by UV−vis flash photolysis in toluene. While such a difference was not observed in the formation of **W**−N_2[36] and **W**−H_2 (see Table 2), this suggests that the interaction of a solvent molecule with the W center may be important in the formation of **W**−C_2H_4. (See Mechanistic Considerations of **W**−L Formation section).

While **W**−py and **W**−$P(OMe)_3$ complexes are more stable than **W**−$NCCH_3$,[9] the stabilities of the various adducts determined in this study are in the order **W**−$NCCH_3$ > **W**−N_2 > **W**−D_2 > **W**−H_2 > **W**−C_2H_4, which match well with the results obtained by Hoff's group[9] for **W**−$NCCH_3$, **W**−N_2, **W**−D_2, and **W**−H_2. Our B3LYP/6-31G** calculations for the model complexes **W′**−L indicate that the **W′**−L binding free energies are in the order **W′**−CO > **W′**−N_2 > **W′**−C_2H_4 > **W′**−H_2 (dihydrogen) > **W′**−*distal*-$(H)_2$ > **W′**−*cis*-$(H)_2$. The fact that **W**−C_2H_4 was found experimentally to be the least stable species, whereas **W′**−C_2H_4 was calculated to have a relatively large binding energy, may be due to a steric factor associated with the bulky Cy groups in **W**−C_2H_4 and the η^2-coordination mode of C_2H_4. In fact, the crystal structure[47] of **W**−C_2H_4 indicates a long W−P distance to accommodate the C═C bond of C_2H_4 parallel to P−W−P.

Isotope Effects. The kinetic isotope effects (KIEs) for the forward and reverse reactions, $k_{f(H_2)}/k_{f(D_2)}$ and $k_{r(H_2)}/k_{r(D_2)}$, for the formation of **W**−L (L = H_2 and D_2), obtained by our photoinduced method, are 1.3 ± 0.2 and 1.4 ± 0.3, respectively, in toluene at 25 °C. The kinetic isotope effect of H_2/D_2 replacement by py obtained by Hoff's group[7] in toluene, $k_{r(H_2)}/k_{r(D_2)} = 1.7 \pm 0.1$, is slightly larger than our H_2/D_2 removal KIE (1.4 ± 0.3). However, these numbers are probably within the respective experimental errors, because our number is estimated from the intercepts (∼10% error) of Figure 3 for the direct binding reactions, while Hoff's value is obtained from estimated rate constants (within ±15% error) using complicated substitution reactions, and also because of the existence of an equilibrium between **W**−H_2 and **W**−$(H)_2$.

Calculated equilibrium constants for **W**−H_2, **W**−D_2, and **W**−C_2H_4 are 2100 ± 300, 2300 ± 300, and 60 ± 10 M^{-1}, respectively. The equilibrium isotope effect (EIE) for the **W** complex has not been directly measured previously, but the equilibrium shown in eq 6 has been used to obtain EIE = $K_H/K_D = 0.70 \pm 0.15$ in THF at 22 °C using calibrated H_2/N_2 and D_2/N_2 gas mixtures.[10] Our value in toluene at 25 °C is 0.91 ± 0.15, which is larger than the value reported.[10] Our preliminary experiments in THF give an EIE of 0.80 ± 0.15 at 15 °C.

$$\mathbf{W}-N_2(\text{soln}) + H_2(g) \rightleftharpoons \mathbf{W}-H_2(\text{soln}) + N_2(g) \qquad (6)$$

K_H/K_D can be calculated from a mass and moment of inertia factor (MMI), a vibrational excitation factor (EXC), and a zero-point energy factor (ZPE) as shown in eq 7.[10,44−46]

$$\text{EIE} = \text{MMI} \times \text{EXC} \times \text{ZPE} \qquad (7)$$

The calculated value (EIE = 0.78)[10] for **W** with H_2/D_2 was in agreement with their experimental value (0.70) and slightly smaller than our experimental values.

Mechanistic Considerations of W−L Formation. When L is photodissociated from **W**−L, a rapid equilibration with the agostic W···H−C interaction of a cyclohexyl group of one of the PCy_3 ligands with the metal center, and possibly a partial coordination of the solvent via a σ C−H interaction of the solvent with the metal center, will take place. The visible spectra in hexane and toluene are identical, indicating that the agostic W···H−C interaction of the cyclohexyl group may be stronger than the σ C−H interaction of solvents. Our calculated free

(41) Perutz, R. N. *Pure Appl. Chem.* **1998**, *70*, 2211−2220.
(42) Mawby, R. J.; Perutz, R. N.; Whittlesey, M. K. *Organometallics* **1995**, *14*, 3268−3274.
(43) Colombo, M.; George, M. W.; Moore, J. N.; Pattison, D. I.; Perutz, R. N.; Virrels, I. G.; Ye, T. Q. *J. Chem. Soc., Dalton Trans.* **1997**, 2857−2859.
(44) Bigeleisen, J.; Goeppert Mayer, M. *J. Chem. Phys.* **1947**, *15*, 261−267.
(45) Bullock, R. M. Isotope Effects in Reactions of Transition Metal Hydrides. In *Transition Metal Hydrides*; Dedieu, A., Ed.; VCH Publishers: New York, 1992; pp 263−307.
(46) Bullock, R. M.; Bender, B. R. Isotope Methods - Homogeneous. In *Encyclopedia of Catalysis*; Horváth, I., Ed.; Wiley and Sons: New York, 2002; pp 281−348.

Table 4. Calculated Binding Energies, Enthalpies, Entropies, and Free Energies for Various **W′**−L, **W**, and Related Complexes

system	L	ΔE (kcal mol^{-1})[a]	$\Delta H°$ (kcal mol^{-1})	$\Delta S°$ (cal K^{-1} mol^{-1})	$\Delta G°_{298}$ (kcal mol^{-1})
binding to $W(CO)_3(PH_3)_2$	CO	−47.6	−45.8	−32.6	−36.1
binding to $W(CO)_3(PH_3)_2$	C_2H_4	−26.9	−25.3	−41.9	−12.8
binding to $W(CO)_3(PH_3)_2$	N_2	−26.0	−24.3	−34.0	−14.2
binding to $W(CO)_3(PH_3)_2$	dihydrogen	−16.8	−14.6	−27.0	−6.5
binding to $W(CO)_3(PH_3)_2$	*distal*-dihydride	−11.2	−9.9	−28.9	−1.2
binding to $W(CO)_3(PH_3)_2$	*cis*-dihydride	−10.5	−9.3	−30.9	−0.9
binding to $W(CO)_3(PH_3)_2$	*n*-hexane	−5.4	−4.4	−32.6	5.3
binding to $W(CO)_5$	*n*-hexane	−7.2	−6.3	−32.1	3.2
net agostic interaction[b] in $W(CO)_3(PCy_3)_2$	agostic α-C−H of PCy_3	−4.7	−5.1	0.6	−5.2
net agostic interaction[b] in $W(CO)_3(PCy_3)(PH_3)$	agostic α-C−H of PCy_3	−5.2	−5.4	−2.1	−4.8
net agostic interaction[b] in $W(CO)_3(PH_3)(PH_2Cy)$	agostic β-C−H of PH_2Cy	−0.5	−0.9	−7.4	1.3

[a] Difference in total electronic energy without correction for zero-point energy. [b] The sum of the intrinsic agostic interaction energy and any steric and/or electronic energy differences associated with the two different conformers.

energy for the formation of **W′**−*n*-hexane ($\Delta G°_{298} = 5.3$ kcal mol^{-1}) indicates that such an interaction may be unfavorable (Table 4). Hoff et al.[9] observed a KIE of 1.20 ± 0.05 for the reaction of **W**−py (and its deuterium-substituted species $W(CO)_3[P(C_6D_{11})_3]_2(py)$) with $P(OMe)_3$ in toluene and verified the importance of the "agostic" W···H−C interaction of a cyclohexyl group in the ligand substitution reaction. This KIE is similar to that of dissociation of py from **W**−py at low py concentrations and indicates that dissociation of py is assisted by partial formation of the C−H agostic bond at the transition state.[8] An inverse KIE of 0.87 for **W** with $P(OMe)_3$ was observed.[8] Again, the agostic interaction must be involved in the transition state.

Kubas' group[47] reported that the static complex, with an agostic W···H−C interaction of a cyclohexyl group of the PCy_3 ligand, does not exist in toluene solution at room temperature due to the fact that the ^{31}P NMR shows only one signal at room temperature and the high-field chemical shift for the agostic hydrogen was not observed. Therefore, the agostic W···H−C interaction of a cyclohexyl group of the PCy_3 ligand was considered to be fluxional. While it is very important to consider the agostic interaction of a cyclohexyl group of the PCy_3 ligand in ligand exchange or addition reactions, the concentration of solvent is much higher than that of the metal species. Therefore, a fluxional interaction of both a solvent molecule and an agostic C−H interaction of a cyclohexyl group with the W center may exist. Such a weak solvent interaction may be important in the reaction of **W** with C_2H_4, in which the rate constant for formation of **W**−C_2H_4 in hexane is 2× faster than that in toluene. We did not observe solvent-dependent rate constants for formation of **W**−L (L = H_2 and N_2). Because the interaction of C_2H_4 with **W** is much weaker than that of the other ligands such as H_2 and N_2 (as evidenced by the much smaller equilibrium constant for the reaction of **W** with C_2H_4), the rate constant in the C_2H_4 experiment is likely to be more noticeably affected by a weaker solvent coordination in hexane, whereas for the other more strongly coordinating ligands, L, the rate constants in hexane are not so perturbed from those measured in toluene. Also, toluene offers the possibility of arene bonding interactions that hexane does not,[48] although such interaction may be relatively weak due to the bulky phosphine groups around the metal center.

To our knowledge, activation volumes for the formation of metal dihydrogen, -dinitrogen, or -ethylene complexes have not been reported. However, those of metal dihydride complexes were determined previously (−20 ± 1 and −16 ± 1 cm^3 mol^{-1} for the formation of $Ir(H)_2Cl(CO)(PPh_3)$ in toluene[49] and $Rh(H)_2(bpy)_2$ in methanol,[19] respectively). The small activation volumes found in the present study (viz., −3, −7, −3, and +3 cm^3 mol^{-1} for the formation of **W**−H_2, **W**−C_2H_4, **W**−N_2, and **W**−$NCCH_3$, respectively) in toluene suggest that **W**−L bond reformation involves the displacement of the fluxional agostic W···H−C interaction of a cyclohexyl group of the PCy_3 ligand and/or toluene in the transition state. These small absolute values therefore result from a combination of bond formation and bond cleavage processes as found in I_a and I_d substitution mechanisms, respectively.

Pulsed laser flash photolysis of $M(CO)_6$ in solution with a known amount of L (M = Cr, Mo, W; L = piperidine, 1-hexene, pyridine, $P(C_6H_5)_3$, $P(OC_2H_5)_3$, etc.) has been investigated in different solvents.[50−53] A rapid formation of $M(CO)_5$(solvent), followed by the displacement of solvent by different entering nucleophiles, L, was observed. For the W complex, small positive activation volumes (0.4−2.7 cm^3 mol^{-1}) are found for L = 1-hexene in fluorobenzene, chlorobenzene, or heptane as a solvent. This was interpreted in terms of a dissociative interchange (I_d) mechanism in which the coordinated solvent is displaced by L. However, when THF was used as a solvent, the reactions of $W(CO)_5$(THF) with piperidine, $P(C_6H_5)_3$, and $P(OC_2H_5)_3$ showed significantly negative activation volumes (−4 to −15 cm^3 mol^{-1}). Thus, in the latter case there is real evidence for an associative type (I_a) mechanism. It is worth pointing out that negative activation volumes were observed in reactions of all metal complexes performed in THF.[50−53] Since THF can bind to $M(CO)_5$ more strongly than any other solvents used in the experiments, an incoming ligand may need to form a partial bond at the transition state, consistent with the I_a mechanism. It seems that the reaction mechanism depends on a balance between the interaction of $W(CO)_5$ with solvents and the nucleophilicity of the incoming ligand.

The photodissociation of L from **W**−L in the present systems can cause a rapid equilibration with the agostic W···H−C

(47) Butts, M. D.; Bryan, J. C.; Luo, X.-L.; Kubas, G. J. *Inorg. Chem.* **1997**, *36*, 3341−3353.
(48) Cheng, T.-Y.; Szalda, D. J.; Bullock, R. M. *J. Chem. Soc., Chem. Commun.* **1999**, 1629−1630.
(49) Schmidt, R.; Geis, M.; Kelm, H. *Z. Phys. Chem.* **1974**, *92*, 223−234.
(50) Zang, V.; Zhang, S.; Dobson, C. B.; Dobson, G. R.; van Eldik, R. *Organometallics* **1992**, *11*, 1154−1158.
(51) Zhang, S.; Dobson, G. R.; Zang, V.; Bajaj, H. C.; van Eldik, R. *Inorg. Chem.* **1990**, *29*, 3477−3482.
(52) Zhang, S.; Zang, V.; Bajaj, H. C.; Dobson, G. R.; van Eldik, R. *J. Organomet. Chem.* **1990**, *397*, 279−289.
(53) Wieland, S.; van Eldik, R. *Organometallics* **1991**, *10*, 3110−3114.

interaction with the metal center, but it could also involve partial coordination of solvent, as found for $M(CO)_5$(solvent) studied previously.[50−53] It is estimated that the energy of the agostic interaction[8,9] is 10 ± 6 kcal mol^{-1} based on a bond strength of 10 kcal mol^{-1} for $Cr(CO)_5$(heptane). Note that the error limit seems to be assigned arbitrarily, but the bond energy is expected to be in the wide range of 4−16 kcal mol^{-1}.[9] Our DFT calculated net agostic interaction energies are $\Delta E = -4.7$ and $\Delta H° = -5.1$ kcal mol^{-1}, which are at the lower end of the estimated range, and are comparable to the binding energy of *n*-hexane ($\Delta H° = -4.4$ kcal mol^{-1}) to **W′**. We should point out that the net agostic C−H interaction of Cy in $W(CO)_3(PCy_3)(PH_3)$ is also rather small ($\Delta H° = -5.4$ kcal mol^{-1}). The displacement reaction with L can follow an associative or dissociative interchange (I_a or I_d) pathway mode, depending on the nucleophilicity of the solvent, agostic interaction, and incoming L. In the case of H_2, N_2, and C_2H_4, the negative activation volumes suggest that bond formation is more important than bond breakage (presumably involving mainly the agostic W···H−C interaction of a cyclohexyl group of a PCy_3 ligand, and possibly the σ bonding interaction of the methyl group of toluene since it is present in huge excess) and favors an I_a substitution mechanism similar to $W(CO)_5$(THF) mentioned above. These results were unexpected for a crowded metal center such as $W(CO)_3(PCy_3)_2$, but there is the precedent that the KIE observed for the reaction of **W**−py with $P(OMe)_3$ verified the involvement of the "agostic" W···H−C interaction of a cyclohexyl group at the transition state in the ligand substitution reaction.[9] In the case of CH_3CN, the positive activation volume suggests that bond cleavage is more important, similar to what was found for $W(CO)_5$(solvent) with 1-hexene in fluorobenzene, chlorobenzene, and heptane solvent as mentioned above. The **W**−$NCCH_3$ complex ($K > 2 \times 10^4$ M^{-1}) is much more stable than **W**−H_2, **W**−N_2, and **W**−C_2H_4. The binding rate constant (3.6×10^6 M^{-1} s^{-1}) of CH_3CN to **W** is the largest we and others have studied using various incoming ligands in toluene. Since CH_3CN is much stronger as an incoming ligand than H_2, N_2, and C_2H_4, the W···H−C agostic interaction and toluene coordination are relatively weak as found for the solvent interaction with $W(CO)_5$ in fluorobenzene, chlorobenzene, and heptane. Therefore, in the CH_3CN case the photogenerated intermediate may follow an I_d substitution mechanism. Thus, our photoproduced intermediate, which we postulate to have a fluxional behavior with W···H−C agostic and possibly **W**−toluene interactions, may behave in a way similar to that found for $M(CO)_5$(solvent) intermediates.

Now let us discuss the likelihood of a solvent σ C−H bonding interaction with **W** vs an agostic interaction in **W** or its transition states for binding a ligand, L, after the photoejection of L from **W**−L. Our $\Delta G°_{298}$ values reflect a large entropy effect favoring an agostic interaction ($-T\Delta S° \approx 0-2$ kcal mol^{-1}) in **W** and disfavoring an interaction of the solvent with **W** ($-T\Delta S° \approx 10$ kcal mol^{-1}). This effect, combined with the small binding energies calculated for the net agostic and σ C−H binding, leads to $\Delta G°_{298}$ for formation of a solvent σ C−H bond with **W** being positive by several kcal mol^{-1}. Small differences (a few kcal mol^{-1}) in $\Delta G°_{298}$, however, could be within the errors associated with the calculations.

Conclusions

In the present study, we investigated, for the first time, direct laser flash photolysis measurements of rate constants and activation volumes for the formation of **W**−L from **W** and L in toluene and hexane solutions containing **W**−L (L = H_2, D_2, C_2H_4, N_2, or CH_3CN) and a known amount of L. **W**−L bond dissociation took place to form **W** and subsequently, clean regeneration of **W**−L was observed by the use of time-resolved UV−vis and s^2-FTIR spectroscopy. The results of the s^2-FTIR experiments demonstrate how TRIR spectroscopy is an extremely powerful technique for probing photoinitiated bond cleavage and formation reactions of transition-metal carbonyl complexes. The data are complementary to those obtained from UV−vis flash photolysis experiments, providing a more accurate spectroscopic picture of the mechanism of the photochemical reaction, thus allowing the simultaneous identification of multiple species and the temporal evolution of each one to be followed. In addition, the high-pressure kinetic data enable a more detailed picture of the ligand exchange process in the transition state to be made. The small negative activation volumes suggest that **W**−L (L = H_2, N_2, or C_2H_4) bond reformation involves the displacement of a fluxional agostic W···H−C interaction of a cyclohexyl group of a PCy_3 ligand and/or the methyl group of toluene in the transition states. DFT calculations have elucidated the nature of the electronic transitions, the assignments of IR frequencies, and bond energies for **W′**−L complexes and **W** species with and without agostic W···H−C interactions. Our DFT calculations indicate an entropy effect that favors agostic W···H−C interaction over a solvent σ C−H interaction by 8−10 kcal mol^{-1}.

Acknowledgment. We thank Dr. Gregory Kubas (Los Alamos National Laboratory) and Professors Michael George (U. Nottingham, UK) and Carl D. Hoff (U. Miami) for insightful suggestions and valuable discussions. We also thank Dr. Bruce S. Brunschwig for his initial assistance in installing the high pressure vessel in the flash photolysis system. This work was performed at Brookhaven National Laboratory, funded under contract DE-AC02-98CH10886 with the U.S. Department of Energy and supported by its Division of Chemical Sciences, Geosciences, & Biosciences, Office of Basic Energy Sciences. RvE gratefully acknowledges financial support from the Deutsche Forschungsgemeinschaft (SFB 583) that enabled his participation in this work.

Supporting Information Available: Pressure-dependent rates for formation of **W**−L, DFT-optimized Cartesian coordinates for 12 W species, plots of rate constants for formation of **W**−L (N_2, C_2H_4, and CH_3CN) in toluene, a rate plot for formation of **W**−C_2H_4 in hexane obtained by s^2-FTIR, and Frontier orbitals for **W′**−C_2H_4; complete ref 29. This material is available free of charge via the Internet at http://pubs.acs.org.

JA064627E